Chinese Chemical Letters 34 (2023) 107945

Contents lists available at ScienceDirect

Chinese Chemical Letters

journal homepage: www.elsevier.com/locate/cclet

High-dimensional zinc porphyrin nanoframeworks as efficient radiosensitizers for cervical cancer

Fei Cai[a,1], Kun Ye[a,1], Mingkai Chen[a,1], Yuan Tian[a], Peicong Chen[b], Hao Lin[b,*], Tianfeng Chen[a], Li Ma[a,*]

[a] Department of Chemistry, Jinan University, Guangzhou 510632, China
[b] Department of Orthopedics, Affiliated Hospital of Guangdong Medical University, Zhanjiang 524001, China

ARTICLE INFO

Article history:
Received 2 August 2022
Revised 17 October 2022
Accepted 24 October 2022
Available online 26 October 2022

Keywords:
Zinc porphyrin frameworks
Nanoframeworks
Radiosensitizer
Apoptosis

ABSTRACT

Radiotherapy is widely used clinically, but the toxic and side effects of nonselective killing of high-energy radiation limit its application. Finding biocompatible materials to assemble radiotherapy sensitizers and studying their sensitization patterns are of great significance for the clinical application. Here, biocompatible zinc porphyrin was chosen as sub-unit to construct various dimensional coordination frameworks. By employing top-down approach, suitable nanoframeworks with various dimensional zinc porphyrin were synthesized as radiosensitizers. The experimental data showed that high-dimensional zinc porphyrin nanoframeworks exhibit higher X-ray response performance.

Radiotherapy is one of the most effective and widely used methods in clinical tumor treatment, but its application is limited due to the toxic and side effects of non-selective killing of high-energy radiation [1]. Therefore, it is urgent to develop high-efficiency and low-toxicity radiosensitizers to reduce the radiation dose while ensuring efficacy [2–4]. We are interested in employing photosensitive ligands and biocompatible metal center to construct sub-unit to further build various dimensional coordination frameworks as radiosensitizers (Fig. 1a) [5–8].

The response efficiency of radiosensitizers to radiation is very critical, and the atomic structure and spatial packing of radiosensitizers are critical to the response efficiency [9–11]. The atomic structure and spatial packing of the radiosensitizer affect the absorption and conversion ability of radiation and the diffusion efficiency of the generated reactive oxygen species (ROS), which ultimately affects the response efficiency [12–15]. Employing the same subunit to construct various-dimensional frameworks as models to investigate the relationship between atomic structure and radiosensitization efficiency is a promising strategy. Herein, we report various dimensional coordination nanosystems with identical sub-unit, mononuclear zinc porphyrin, tetranuclear zinc porphyrin, one-dimensional zinc porphyrin chain and three-dimensional zinc porphyrin framework, used as radiosensitizers for cervical cancer treatment (Fig. 1b).

As an important component of chlorophyll, porphyrins is a large aromatic system [16,17], with high photosensitivity [18], tumor selectivity [19,20], and stable metal ion coordination ability [21,22], which is an excellent choice for the construction of radiosensitizers [23–25]. Zinc is an essential trace element for the human body and the active center of zinc enzymes [26–28], which plays a vital role in maintaining the structure and the activity of enzymes [29–31]. In this work, 5,10,15,20-tetra(4-pyridyl)porphyrin (TPyP-H_2) was employed as the ligand to construct the zinc porphyrin sub-unit, and the pyridyl axis coordinated the zinc ion to construct the framework with various dimensions. The experimental data showed that nanoframeworks with different dimensional exhibit different response efficiencies, and high-dimensional nanoframeworks exhibit higher X-ray response performance (Fig. 1c).

To ensure that nanosystems are coordinated frameworks of different dimensions at the microscopic scale, a top-down synthesis approach is employed to obtain suitable nanomaterials with similar sizes and defined coordination frameworks [32–35]. Firstly, in order to obtain defined coordination frameworks, various methods were used to synthesize and obtain crystals suitable for single-crystal diffraction by using TPyP-H_2 and zinc salts. By reacting at room temperature in methanol, mononuclear zinc porphyrin (Zn0D) was obtained with $TPyP^{2-}$ as tetradentate ligand coordinated to zinc metal using four nitrogen atoms in porphyrin ring. Using Zn0D as a sub-unit, different dimensional coordination frameworks were synthesized by solvothermal method under vari-

* Corresponding authors.
E-mail addresses: puningworker@163.com (H. Lin), chem_mali@jnu.edu.cn (L. Ma).
[1] These authors contributed equally to this work.

https://doi.org/10.1016/j.cclet.2022.107945
1001-8417/

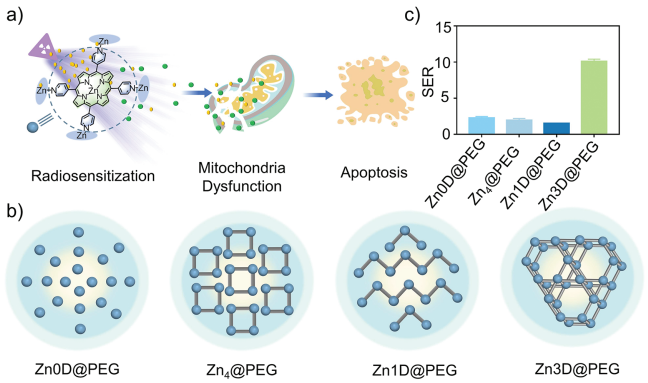

Fig. 1. (a) Schematic representation of zinc porphyrin nanoframeworks used as efficient radiosensitizers. (b) Schematic representation of the synthesized different dimensional zinc porphyrin nanoframeworks. (c) The sensitizer enhancement ratio (SER) IC_{50} of Zn0D@PEG, Zn_4@PEG, Zn1D@PEG and Zn3D@PEG under 4 Gy X-ray irradiation. The SER was calculated by MTT assay.

ous conditions. The single crystal X-ray diffraction analysis showed that through one or more pyridyl group in $TPyP^{2-}$ axis coordinated the zinc ion tetranuclear zinc porphyrin (Zn_4), one-dimensional zinc porphyrin chain (Zn1D) and three-dimensional zinc porphyrin framework (Zn3D) were constructed (Fig. S1 and Tables S1-S3 in Supporting information). The crystal structure of the Zn porphyrin framework in three different dimensions clearly shows the coordination mode of the porphyrins with Zn. Zn_4 consists of four zinc porphyrins oriented almost vertically, converging into a square tetrameric point, which belongs to the $P4_2/n$ space group, monoclinic; each Zn ion in Zn1D has a square pyramidal coordination geometry with the four equatorial N atoms of the porphyrin ligand. In Zn3D, the Zn ion is in a six-coordination mode, so that after binding to a porphyrin in the plane, it also binds to the N atom of the adjacent porphyrin in the axis, thus forming a three-dimensional structure in a three-dimensional interlocking pattern, belonging to the tripartite crystal system, R-3 space group. The purity of the three crystals was checked by powder X-ray diffraction analysis (Fig. S2 in Supporting information).

Furthermore, the scale of a material is closely related to its biological effect, and the difference in scale affects the absorption [36] and pharmacology [35] of drugs. To exclude the effect of size while improving the cellular uptake and circulation time of the zinc porphyrin frameworks, we nanolized the materials through top-down approach by ultrasonic crushing [37–39]. After ultrasonic crushing, the various dimensional frameworks were scaled down to similar nanoscale, around 200 nm (Fig. 2a). In order to stabilize the nanolized nanoframeworks, PEG, a nontoxic water-soluble surfactant without strong coordination atoms, was employed to construct the nanosystems, Zn0D@PEG, Zn_4@PEG, Zn1D@PEG and Zn3D@PEG (Fig. 1b). The TEM-EDS mapping (Fig. 2b) and powder X-ray diffraction analysis (Fig. 2c) results further confirmed the original coordination frameworks were maintained in the nanoframeworks. These results confirmed that we have obtained suitable nanomaterials with similar sizes and defined various dimensional coordination frameworks.

In order to investigate the radiotherapy sensitivity of the different dimensional nanoframeworks (Fig. 3a), an *in vitro* evaluation was performed using the (3-(4,5-dimethylthiazol-2-yl)−2,5-diphenyltetrazolium bromide) tetrazolium (MTT) assay to evaluate their cytotoxicity and radiosensitization effect. Prior to evaluate of cellular events, the stability of these nanoframworks in solution and under X-ray radiation was established by UV–vis spectroscopy. As shown in Fig. 3b and Fig. S3 (Supporting information), the size of the nanoframeworks did not change much with time, and the nanoframeworks was not damaged after X-ray radiation, indicating that the nanoframeworks have good stability.

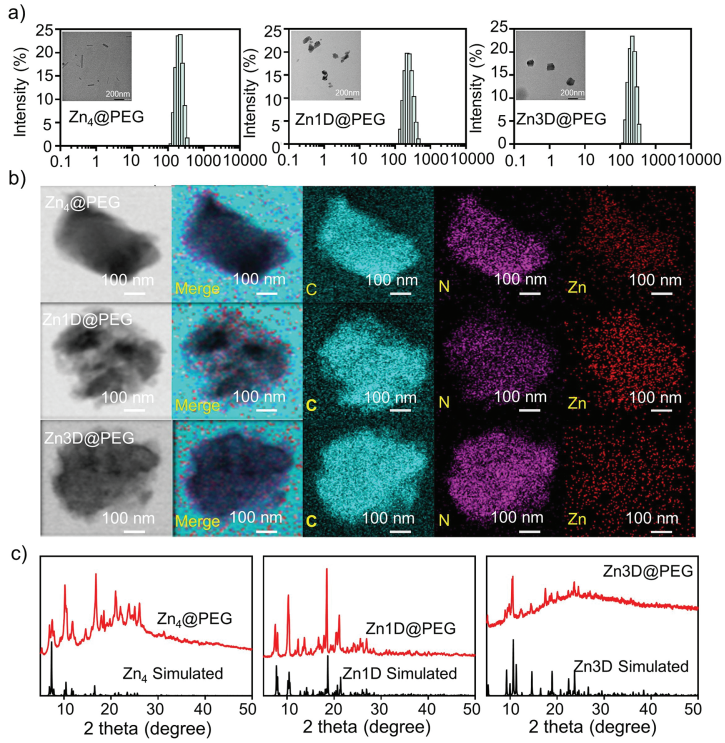

Fig. 2. Characterization of the synthesized different dimensional zinc porphyrin nanoframeworks. (a) Dynamic light scattering (DLS) spectrum of nanoframeworks. The inserts are the TEM images of the corresponding nanoframeworks (scale bar: 200 nm). (b) Mapping diagram of energy spectrum analysis of nanoframeworks. (c) PXRD patterns of nanoframeworks. The below black lines are PXRD patterns simulated based on the single crystal X-ray diffraction data. The above red lines are PXRD patterns for the synthesized nanoframeworks.

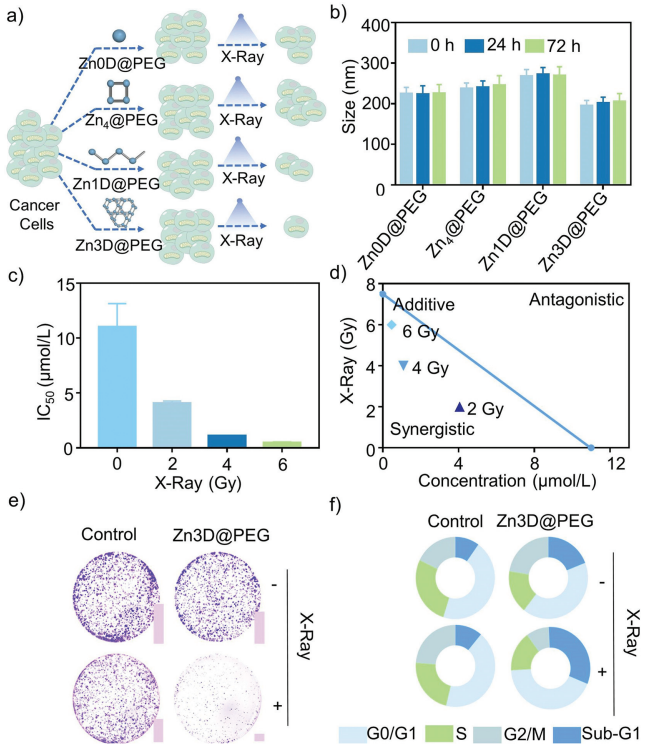

Fig. 3. Nanoframeworks as radiosensitizers to enhance radiotherapy. (a) Schematic illustration of the radiosensitization efficiency of the synthesized different dimensional nanoframeworks. (b) The stability of the nanoframeworks detected by DLS. (c) The IC_{50} of Zn3D@PEG with/without radiation on HeLa cells. (d) Isobologram analysis of the synergistic antiproliferative effect of the combined treatment of X-ray and Zn3D@PEG on HeLa cells. (e) Clone formation photographs of HeLa cells under the co-treatment of 6 μmol/L Zn3D@PEG and X-ray. (f) Flow cytometric analysis of the effect by Zn3D@PEG (6 μmol/L) with/without X-ray treating in HeLa cell cycle distribution for 72 h.

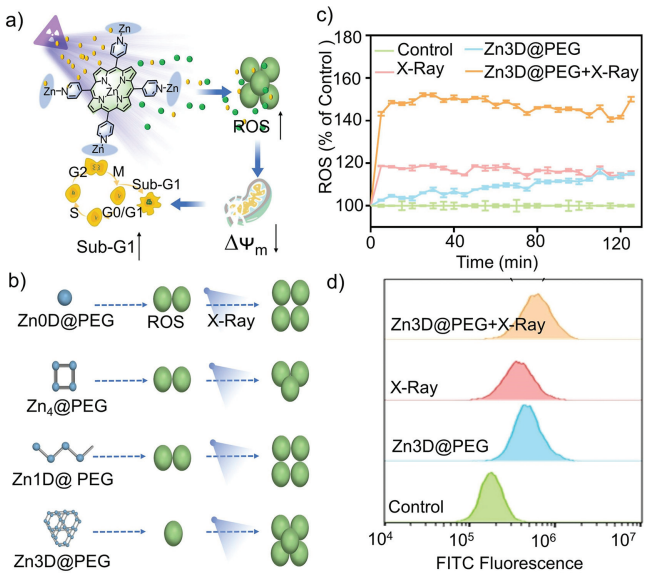

Fig. 4. (a) Schematic diagram of anticancer mechanism of co-treatment of drugs and X-ray. (b) Schematic diagram of ROS levels after various treatment. (c) Intracellular ROS changes of HeLa cells by co-treatment of 12 μmol/L Zn3D@PEG and X-ray. (d) Mitochondrial membrane potential in HeLa cells after the treatment with 12 μmol/L Zn3D@PEG and X-ray for 48 h.

Next, the MTT method was used to assay the anti-cancer activity of different dimensional zinc porphyrin nanoframeworks against cervical cancer cell lines (HeLa, SiHa) and human cervical epithelial cell line (Ect1/E6E7) was selected as reference. As shown in Table S4 (Supporting information), these nanosystems of different dimensional frameworks showed similar anticancer effects with IC_{50} values (concentration required to inhibit half-cell growth) of approximately 10 μmol/L. Combined with X-ray co-treatment (Fig. 3c and Fig. S4 in Supporting information), the IC_{50} values decreased obviously in a dose-dependent manner. Isobologram analysis was employed to study the interaction between nanoframeworks and X-ray (Fig. 3d and Fig. S4). As shown in the isobologram, all the data points below the additive effect line, which means that the co-treatment of nanoframeworks and X-ray results in a synergistic effect. In order to further verify the effect of the combined treatment of Zn3D@PEG and X-ray, the colony formation assay was used to detect the growth of the HeLa cell population after the combined treatment. As shown in Fig. 3e, the combined treatment of Zn3D@PEG and X-ray well inhibited the formation of cell populations, which further verified the good sensitization effect of Zn3D@PEG on radiotherapy.

Furthermore, from the co-treatment results of various dimensional zinc porphyrin nanoframeworks and X-ray (Fig. 3c and Fig. S4), we can see that nanoframeworks with high-dimension structures show higher X-ray responsiveness. This is probably because the three-dimensional nanoframeworks (Zn3D@PEG) is the most rigid system and a smaller proportion of the energy received is dissipated as heat [40]. On the other hand, there are pores in the three-dimensional framework of zinc porphyrin, which is conducive to the diffusion of the generated ROS, so the radiosensitization effect is better. Then we further analyzed the cell cycle profile induced by co-treatment by flow cytometry. As shown in Fig. 3f and Fig. S5 (Supporting information), after combined treatment, the peak value of Sub-G1 was significantly higher than that of the control group, from 9.56% to 31.24% (Fig. S6 in Supporting information), and there were no significant changes in other cell cycles. This suggests that the combination treatment induces cell apoptosis, thereby sensitizing radiotherapy, possibly due to the large amount of ROS generated that may first lead to mitochondrial dysfunction, the main organelle for ROS production [41,42] which ultimately kills tumor cells (Fig. 4a).

In order to further investigate the detailed action mechanism, a DCFH-DA probe (dichloro-dihydro-fluorescein diacetate) was used to detect the intracellular changes of ROS after zinc porphyrin nanoframeworks and X-ray co-treatments. As shown in Fig. 4b, all the co-treatment increased the production of ROS, especially the high-dimensional nanoframeworks. As shown in Fig. 4c and Fig. S7 (Supporting information), the ROS increased to approximately 110% in the Zn3D@PEG-treated group, and further increased to around 150% combined radiotherapy compared with the control group. Excessive intracellular ROS can damage mitochondria, leading to mitochondrial dysfunction and further apoptosis [43,44]. To confirm mitochondrial function, the mitochondrial membrane potential indicator JC-1 was used to detect mitochondrial damage by Zn3D@PEG and X-ray co-treatment. As shown in Fig. 4d and Fig. S8 (Supporting information), a concentration-dependent increase in green fluorescence was found in HeLa cells treated with Zn3D@PEG (6 μmol/L) alone, from 0.70% to 27.52%, which further increased to 57.28% after X-ray co-treatment, indicating that the combination of Zn3D@PEG with X-ray induced mitochondria dysfunction.

Taken together, the co-treatment produced a large amount of ROS, leading to mitochondria dysfunction and increased cell apoptosis, which ultimately killed cancer cells.

In conclusion, we constructed zinc porphyrin sub-units using photosensitive porphyrin ligand and essential trace element zinc, and then synthesized various dimensional zinc porphyrin coordination frameworks. Through top-down approach nanolizing

the framework, suitable for radiosensitization nanoframeworks are obtained for further study. The experimental data showed that nanoframeworks with different dimensional exhibit different response efficiencies, and high-dimensional nanoframeworks exhibit higher X-ray response performance. This is probably because the high-dimensional nanoframeworks is the most rigid system and a smaller proportion of the energy received is dissipated as heat. The co-treatment of the synthesized nanoframeworks and X-ray produced a large amount of ROS, leading to mitochondria dysfunction and increased cell apoptosis, which ultimately killed cancer cells. Overall, this work provides a valuable reference for subsequent researchers to develop high-efficiency and low-toxicity radiosensitizers.

Declaration of competing interest

The authors declare that they have no known competing financial interests or personal relationships that could have appeared to influence the work reported in this paper.

Acknowledgments

This work was supported by National Natural Science Foundation of China (Nos. 21877049, 22177038, 32171296), Guangdong Natural Science Foundation (Nos. 2020B1515120043, 2022A1515012235), Major Program for Tackling Key Problems of Industrial Technology in Guangzhou (Nos. 201902020013), Guangdong Pearl River Talent Program (No. 2017GC010354), Innovation Team Project in Guangdong Colleges and Universities (Nos. 2019KCXTD008, 2019KTSCX012).

Supplementary materials

Supplementary material associated with this article can be found, in the online version, at doi:10.1016/j.cclet.2022.107945.

References

[1] Y. Chong, J. Ning, S. Min, J. Ye, C. Ge, Chin. Chem. Lett. 33 (2022) 3315–3324.
[2] Y. Chen, P. Gao, T. Wu, et al., Chem. Commun. 56 (2020) 10621–10630.
[3] N. Goswami, Z. Luo, X. Yuan, D.T. Leong, J. Xie, Mater. Horiz. 4 (2017) 817–831.
[4] R. Zhao, H. Liu, Y. Li, M. Guo, X.D. Zhang, Bioconjug. Chem. 32 (2021) 411–429.
[5] S. Hiroto, Y. Miyake, H. Shinokubo, Chem. Rev. 117 (2017) 2910–3043.
[6] C.M. Lemon, P.J. Brothers, B. Boitrel, Dalton Trans. 40 (2011) 6591–6609.
[7] B. Marydasan, R.R. Nair, P.S.S. Babu, D. Ramaiah, S.A. Nair, ACS Omega 4 (2019) 12808–12816.
[8] H.H. Wang, H.Y. Liu, F. Cheng, et al., Chin. Chem. Lett. 29 (2018) 1404–1408.
[9] M. Overchuk, M. Zheng, M.A. Rajora, et al., ACS Nano 13 (2019) 4560–4571.
[10] M.A. Rajora, J.W.H. Lou, G. Zheng, Chem. Soc. Rev. 46 (2017) 6433–6469.
[11] Y. Wu, J.C. Liu, R.Z. Li, C.G. Ci, Polyhedron 211 (2022) 11573.
[12] G. Song, L. Cheng, Y. Chao, K. Yang, Z. Liu, Adv. Mater. 29 (2017) 1700996.
[13] K. Ni, G. Lan, C. Chan, et al., Matter 1 (2019) 1331–1353.
[14] B. Ortiz-Casas, A. Galdámez-Martínez, J. Gutiérrez-Flores, et al., Mater. Today 50 (2021) 533–569.
[15] W. Zhou, Z. Liu, N. Wang, et al., ACS Omega 7 (2022) 12021–12029.
[16] T.S. Balaban, M. Linke-Schaetzel, A.D. Bhise, N. Vanthuyne, C. Roussel, Eur. J. Org. Chem. 18 (2004) 3919–3930.
[17] N. Zhang, L. Wang, H. Wang, et al., Nano Lett. 18 (2018) 560–566.
[18] R.D. Mukhopadhyay, Y. Kim, J. Koo, K. Kim, Acc. Chem. Res. 51 (2018) 2730–2738.
[19] J.M. Park, K.I. Hong, H. Lee, W.D. Jang, Acc. Chem. Res. 54 (2021) 2249–2260.
[20] C. Li, Z. Luo, L. Yang, et al., Mater. Today Bio 13 (2022) 100198.
[21] P. Ling, C. Qian, J. Yu, F. Gao, Chem. Commun. 55 (2019) 6385–6388.
[22] Y. Zhou, X. Liang, Z. Dai, Nanoscale 8 (2016) 12394–12405.
[23] J. Chen, T. Fan, Z. Xie, et al., Biomaterials 237 (2020) 119827.
[24] N. Rabiee, M.T. Yaraki, S.M. Garakani, et al., Biomaterials 232 (2020) 119707.
[25] Z. Luksiene, P. Juzenas, J. Moan, Cancer Lett. 235 (2006) 40–47.
[26] F. Shi, J. Xu, Z. Hu, et al., Chin. Chem. Lett. 32 (2021) 3185–3188.
[27] Y. Zhang, X. Han, Y. Liu, et al., Mater. Adv. 3 (2022) 3709–3725.
[28] K. Ding, Y. Zhang, W. Si, et al., ACS Appl. Mater. Interfaces 10 (2018) 238–247.
[29] K. Lim, S.I. Cho, J.S. Kim, Nat. Commun. 13 (2022) 366.
[30] Q. Chen, K. Ma, X. Liu, et al., Cell Discov. 8 (2022) 3.
[31] S. Sun, Z. Zhang, Y. Xiang, M. Cao, D. Yu, Langmuir 38 (2022) 1621–1630.
[32] J. Cremers, R. Haver, M. Rickhaus, et al., J. Am. Chem. Soc. 140 (2018) 5352–5355.
[33] J. Li, L. Zeng, Z. Wang, et al., Adv. Mater. 34 (2022) 2100245.
[34] M.D. Peeks, C.E. Tait, P. Neuhaus, et al., J. Am. Chem. Soc. 139 (2017) 10461–10471.
[35] D. Yang, S. Zuo, H. Yang, et al., Adv. Mater. 34 (2022) 2107293.
[36] B. Lei, M. Wang, Z. Jiang, et al., ACS Appl. Mater. Interfaces 10 (2018) 16698–16706.
[37] F. Gong, N. Yang, X. Wang, et al., Nano Today 32 (2020) 100851.
[38] T.F. Fu, L. Ao, Z.C. Gao, X.L. Zhang, F. Wang, Chin. Chem. Lett. 27 (2016) 1147–1154.
[39] J. Wu, T. Hu, G. Zhao, A. Li, R. Liang, Chin. Chem. Lett. 33 (2022) 4437–4448.
[40] T. Luo, Y. Fan, J. Mao, et al., J. Am. Chem. Soc. 144 (2022) 5241–5246.
[41] I. Romero-Canelon, P.J. Sadler, Inorg. Chem. 52 (2013) 12276–12291.
[42] C. Liu, X. Xu, J. Zhou, et al., BMC Mater. 2 (2020) 7.
[43] Q. Chen, Y.C. Chai, S. Mazumder, et al., Cell Death Differ. 10 (2003) 323–334.
[44] Y. Dai, Y. Ding, L. Li, Chin. Chem. Lett. 32 (2021) 2715–2728.